






Synapse topology and downmodulation events determine the functional outcome of anti-CD19 T cell-redirecting strategies

Ángel Ramírez-Fernández ^{a,b,#}, Óscar Aguilar-Sopeña ^{c,d,#}, Laura Díez-Alonso^{a,b}, Alejandro Segura-Tudela^{a,b}, Carmen Domínguez-Alonso^{a,b}, Pedro Roda-Navarro ^{c,d}, Luis Álvarez-Vallina ^{a,b,e}, and Belén Blanco ^{a,b,e}

^aCancer Immunotherapy Unit (UNICA), Department of Immunology, Hospital, Universitario 12 de Octubre, Madrid, Spain; ^bImmuno-Oncology and Immunotherapy Group, Instituto de Investigación Sanitaria 12 de Octubre (imas12), Madrid, Spain; ^cDepartment of Immunology, Ophthalmology and ENT, School of Medicine, Universidad Complutense, Madrid, Spain; ^dLymphocyte Immunobiology Group, Instituto de Investigación Sanitaria 12 de Octubre (imas12), Madrid, Spain; ^eRed Española de Terapias Avanzadas (TERAV), Instituto de Salud Carlos III (RICORS, RD21/0017/0029), Madrid, Spain

ABSTRACT

Cancer immunotherapy strategies based on the endogenous secretion of T cell-redirecting bispecific antibodies by engineered T lymphocytes (STAb-T) are emerging as alternative or complementary approaches to those based on chimeric antigen receptors (CAR-T). The antitumor efficacy of bispecific anti-CD19 × anti-CD3 (CD19×CD3) T cell engager (BiTE)-secreting STAb-T cells has been demonstrated in several mouse models of B-cell acute leukemia. Here, we have investigated the spatial topology and downstream signaling of the artificial immunological synapses (IS) that are formed by CAR-T or STAb-T cells. Upon interaction with CD19-positive target cells, STAb-T cells form IS with structure and signal transduction, which more closely resemble those of physiological cognate IS, compared to IS formed by CAR-T cells expressing a second-generation CAR bearing the same CD19-single-chain variable fragment. Importantly, while CD3 is maintained at detectable levels on the surface of STAb-T cells, indicating sustained activation mediated by the secreted BiTE, the anti-CD19 CAR was rapidly downmodulated, which correlated with a more transient downstream signaling. Furthermore, CAR-T cells, but not STAb-T cells, provoke an acute loss of CD19 in target cells. Such differences might represent advantages of the STAb-T strategy over the CAR-T approach and should be carefully considered in order to develop more effective and safer treatments for hematological malignancies.

ARTICLE HISTORY

Received 4 November 2021
Revised 23 February 2022
Accepted 11 March 2022

KEYWORDS

CD19⁺ B cell malignancies; T cell-redirecting strategies; STAb; BiTE; CAR; leukemia relapse

Introduction

In the past few years, immunotherapeutic strategies based on the redirection of T cells toward cell-surface tumor-associated antigens (TAAs), such as adoptive cellular therapy with chimeric antigen receptor (CAR)-modified T cells or administration of bispecific antibodies (bsAbs), have revolutionized the treatment landscape of hematologic malignancies.¹ CARs are synthetic receptors consisting of an extracellular antigen-binding domain, usually a single-chain fragment variable (scFv) antibody, a transmembrane domain, and a T cell-activating domain, most often the intracellular signaling region of the CD3 linked to a costimulatory sequence (from CD28 or 4-1BB molecules).² Four anti-CD19 CAR-T cell therapies³⁻⁵ and one anti-BCMA (B cell maturation antigen) CAR-T cell therapy⁵ have been approved by the US Food and Drug Administration (FDA) for the treatment of patients with relapsed or refractory (R/R) B cell malignancies and multiple myeloma, respectively. Despite high complete response rates, 30–60% of patients relapse after anti-CD19 CAR-T cell therapy⁶ and its application in solid tumors remains challenging.⁷


BsAbs are artificial molecules designed to bridge two different epitopes, usually a cell surface TAA and the CD3 chain of the TCR/CD3 complex,⁸ resulting in T cell cytokine secretion

and cytotoxic effector functions.^{8,9} An anti-CD19 × anti-CD3 bispecific T cell engager (BiTE), blinatumomab, has been approved by the FDA for the treatment of R/R and minimal residual disease-positive B-cell acute lymphoblastic leukemia (B-ALL).^{10,11} A potential advantage of bsAbs over CAR-T cells is their ability to achieve the polyclonal recruitment of bystander T cells. However, the need for continuous intravenous administration to overcome their short serum half-life¹² and their inability to actively traffic to tumors^{13,14} represent major disadvantages compared to CAR-T therapy.¹ In addition, despite the impressive responses observed with blinatumomab,^{13,15,16} 44% of patients relapse after initial response.¹⁴

Although no clinical data directly comparing CAR-T cells and blinatumomab treatments are available, data suggest that CAR-T cells achieve greater antitumor efficacy and a more prolonged antileukemic response,^{17,18} presumably due to their long-term persistence (up to 39 months).³ By contrast, blinatumomab short half-life is associated with shorter relapse-free survival.¹⁸ Moreover, CAR-T therapy has been proved to be more efficient than blinatumomab in patients with high tumor burden or with extramedullary disease (EMD),¹⁸

CONTACT Belén Blanco  bblanco.imas12@h12o.es  Cancer Immunotherapy Unit (UNICA), Department of Immunology, Hospital Universitario 12 de Octubre, Avenida de Córdoba s/n, 28041 Madrid, Spain; Pedro Roda-Navarro  proda@med.ucm.es; Luis Álvarez-Vallina  lav.imas12@h12o.es

[#]These authors contributed equally

 Supplemental data for this article can be accessed on the [publisher's website](#)

© 2022 The Author(s). Published with license by Taylor & Francis Group, LLC.

This is an Open Access article distributed under the terms of the Creative Commons Attribution-NonCommercial License (<http://creativecommons.org/licenses/by-nc/4.0/>), which permits unrestricted non-commercial use, distribution, and reproduction in any medium, provided the original work is properly cited.

which could be related to the potential of CAR-T cells to actively traffic to extramedullary leukemia deposits,¹⁸ whereas there is no evidence of blinatumomab's ability to cross the blood–brain barrier.¹⁸ In addition, higher complete response rates in pediatric patients have been achieved with CAR-T treatment.¹⁷

In an attempt to overcome the drawbacks and combine the advantages of both strategies, another immunotherapy approach, based on the *in situ* secretion of T cell-redirecting bsAbs (STAb) by genetically modified T cells, is emerging. Thus, *in vivo* secretion of the T cell-redirecting bsAb might result in constant effective concentrations, compensating for the rapid renal clearance of small-sized antibody fragments¹⁹ and, importantly, in STAb strategies T cell recruitment is not restricted to engineered T cells, as in the case of CAR-T cell approaches. The polyclonal recruitment by bsAbs of both engineered and unmodified bystander T cells, present at the tumor site, might lead to a significant boost in antitumor T cell responses.²⁰ We and others have previously shown that STAb-T cells mediate potent antitumor responses *in vivo* in several animal models,^{21–24} but whether the STAb-T strategy might be more effective than CAR-T therapy has remained poorly studied. In particular, a relevant issue concerns the structure of the immune synapse (IS) formed by the CAR-TAA or bsAbs-TAA interactions. It has been reported that the IS initiated by CARs exhibits major differences to the canonical TCR-initiated IS in effector T cells, conforming a disorganized multifocal signaling cluster structure and giving rise to shorter interactions,^{25–28} but further studies are needed to more precisely define the impact of non-classical IS in the functional capacity and cytotoxic potential of CAR-T cells. Contrary to CARs, Fc-free T cell-redirecting bsAbs are able to induce the formation of a classical IS between T cells and tumor cells.²⁹ Indeed, BiTE-initiated IS has been reported to be identical in structure and molecular composition to TCR-induced IS.^{30,31}

We have recently demonstrated that engineered primary human T cells secreting a CD19xCD3 bsAb (STAb-T19) are more effective than engineered T cells bearing a second-generation CAR with the same anti-CD19 clone (CAR-T19) in several *in vivo* models of B-ALL.²⁸ Interestingly, we observed that the secreted BiTE mediated the organization of a canonical IS between primary T cells and CD19⁺ cells, whereas CAR-T19 cells formed a noncanonical and disorganized IS.²⁸ Here, we have further studied the topology of the IS induced by both anti-CD19 T cell-redirecting strategies, with special emphasis on the expression and dynamics of relevant molecules for cell signaling and activation.

Material and methods

Cell lines and culture conditions

HEK293T (CRL-3216) cells were cultured in Dulbecco's modified Eagle's medium (DMEM) (Lonza, Walkersville, MD, USA) supplemented with 2 mM L-glutamine (Life Technologies, Paisley, UK), 10% (vol/vol) heat-inactivated fetal bovine serum (FBS), and antibiotics (100 units/mL penicillin, 100 µg/mL streptomycin) (both from Sigma-Aldrich, St. Louis, MO, USA), referred to as DMEM complete medium

(DCM). Jurkat Clone E6-1 (TIB-152), Raji (CCL-86), and NALM6 (CRL3273) (CCL243) cells were maintained in RPMI-1640 (Lonza) supplemented with 2 mM L-glutamine, heat-inactivated 10% FBS, and antibiotics, referred to as RPMI complete medium (RCM). All cell lines were obtained from the American Type Culture Collection (Rockville, MD, USA) and were grown at 37°C and 5% CO₂. All cell lines were routinely screened for mycoplasma contamination by PCR using the Mycoplasma Gel Detection Kit (Biotools, Madrid, Spain).

Preparation of lentiviral particles and transduction

The lentiviral vectors pCCL-EF1α-BiTE19,²⁸ containing the human kappa light chain signal peptide L1,³² the A3B1 scFv (VL-VH),³³ a five-residue linker (G4S), the OKT3 scFv (VH-VL)³⁴ and a C-terminal polyHis tag, and pCCL-EF1-CAR19,³³ encoding a second-generation (CD8-BBζ) anti-CD19 CAR (19-CAR),³³ was used. To produce lentiviral particles, HEK293T cells were transfected with the transfer vector (pCCL-EF1α-BiTE19 or pCCL-EF1-CAR19) together with packaging plasmids. In brief, HEK293T cells (6×10^6) were plated 24 hours before transfection in 10 cm dishes. At the time of transfection, 6.9 µg transfer vector (pCCL-EF1α-BiTE19 or pCCL-EF1α-CAR19), 3.41 µg pMDLg/pRRE (Addgene, 12251), 1.7 µg pRSV-Rev (Addgene, 12253), and 2 µg envelope plasmid pMD2.G (Addgene, 12259) were diluted in serum-free DMEM. 35 µg linear polyethyleneimine (PEI) molecular weight 25,000 (Polysciences, 23966–1) was added to the mixture and incubated for 20 minutes at room temperature. After incubation, DNA-PEI complexes were added onto the cells cultured in 7 mL of complete DMEM. Media were replaced 4 hours later.

Viral supernatants were collected 48 hours later and clarified by centrifugation and filtration using a 0.45-µm filter. Viral supernatants were concentrated using ultracentrifugation at 26,000 rpm for 2 hours 30 minutes. Virus-containing pellets were resuspended in complete XVivo15 media (Lonza, Walkersville, MD, USA) and stored at –80°C until use.

Functional titers (TU/ml) were determined by FACS analysis after limiting dilution in Jurkat cells, as specified in the flow cytometry section. Jurkat cells at a concentration of 1×10^6 cells/ml cells were left untransduced (nontransduced, J-NT-T cells) or transduced with 19-CAR (J-CAR-T19 cells) or 19-BiTE (J-STAb-T19 cells) encoding lentivirus at the indicated Multiplicity of Infection (MOI). A period of cell expansion of 6–8 days was carried out before conducting experiments.

Viral copy number

The copy number of integrated lentiviruses in J-NT-T, J-CAR-T19, and J-STAbT19 cells was determined by qPCR with the Lenti-X Provirus Quantitation kit (Takara Bio Inc, Saint Germain, France) following the manufacturer's instructions.

Western blotting

For analysis of CAR and BiTE expression, samples were lysed for 5 minutes in an ice-cold RIPA buffer (Sigma-Aldrich) with 5 mM EDTA and a 1x Halt Protease Inhibitor Cocktail

(ThermoFisher-Pierce Biotechnology, Rockford, IL, USA), centrifuged at 11,000 g for 10 minutes at 4°C and soluble fractions were collected; for analysis of BiTE secretion, culture supernatants were collected. 15 µg of protein or 16 µl of supernatant were separated under reducing conditions on 10–20% Tris-glycine gels (Life Technologies, Carlsbad, CA, USA), transferred onto Immobilon-PVDF membranes (Merck Millipore, Tullagreen, Carrigtwohill, Ireland) and probed with mouse antihuman CD247 mAb (1:1000) (BD Biosciences) or anti-His mAb (Qiagen, Hilden, Germany) (200 ng/ml), followed by incubation with horseradish peroxidase (HRP)-conjugated goat antimouse (GAM) IgG, Fc specific (1:5000) (Sigma-Aldrich).

HRP-conjugated mouse anti-actin mAb (1:50,000) was used as loading control. Visualization of protein bands was performed with Pierce ECL Western Blotting substrate. Blots were scanned and quantified using a Bio-Rad ChemiDoc MP Imaging System.

For analysis of T cell signaling, J-CAR-T19 and J-STAb-T19 cells were incubated at 37°C with Raji cells at a Jurkat-Raji ratio of 10:1 for the indicated times. J-NT-T cells were incubated with non-loaded Raji cells or Raji cells loaded for 1 hour with 5 nM blinatumomab (BLI) (Amgen Inc, Thousand Oaks, California) or 1 µg/mL *Staphylococcus aureus* Enterotoxin-E (SEE) (Toxin Technologies, Sarasota, FL, USA). The stimulation time 0 minutes corresponds to J-NT-T cells mixed with Raji cells at room temperature, which were immediately centrifuged and lysed. Samples were lysed for 30 minutes in an ice-cold lysis buffer containing 20 mM Tris-HCl pH 7.5; 1% NP-40; 0.2% Triton X-100 (Sigma-Aldrich); 2 mM EDTA; 150 mM NaCl; 1.5 mM MgCl₂; 5 mM β-glycerolphosphate; 1x protease inhibitor cocktail; 1 mM NaF; 1 mM PMSF; 1 mM Na₃VO₄ and 1 mM Sodium pyrophosphate. Lysates were then centrifuged at 10,000 rpm for 10 minutes at 4°C, and soluble fractions were collected, mixed with 6x Laemmli buffer (Alfa Aesar, Haverhill, MA, USA) containing 20% β-mercaptoethanol, boiled at 95°C for 5 minutes, and resolved in 10% SDS-PAGE acrylamide gels. Resolved proteins were transferred to Immobilon PVDF membranes, which were blocked with blocking buffer (LI-COR Bioscience, Lincoln, NE, USA), incubated overnight with rabbit anti-phospho-Y783-PLCγ1, anti-PLCγ1, anti-phospho-T202/T204-ERK1/2, or mouse anti-ERK1/2 primary antibodies (all from Cell Signaling Technology, Beverly, MA, USA) and incubated for 30 minutes with IRDye 680-conjugated goat-antirabbit (GAR) and IRDye 800-conjugated GAM (Miltenyi Biotec). All blots were scanned, and fluorescence was quantified with an Odyssey Infrared Imager (LI-COR). Densitometry of images was done with Image Studio Freeware (LI-COR). When necessary, blots were striped in 50 ml containing 2% SDS; 12.5% Tris-HCl pH 6.8 and 0.7% β-mercaptoethanol for 30 minutes at 50°C.

Flow cytometry

The following mAbs against human proteins were used: PE-conjugated anti-CD2 (clone S5.2), APC-conjugated anti-CD3 (clone UCHT1), and APC-conjugated anti-CD10 (clone HI10a) from BD Biosciences (San Jose, CA, USA) and PC7-conjugated anti-CD19 (clone J4.119) from Beckman Coulter

(Marseille Cedex, France). DAPI (SigmaAldrich) was used as a viability marker. Cell surface expression of 19-CAR was analyzed using an APC-conjugated GAM IgG F(ab')₂ (Jackson ImmunoResearch, West Grove, PA, USA). Cell surface-bound 19-BiTE was detected with APC-conjugated anti-His mAb (clone GG11-8F3.5.1, Miltenyi Biotec), and intracellular BiTE was detected with APC-conjugated anti-His mAb after cell fixation and permeabilization with Inside Stain kit (Miltenyi Biotec). Cell acquisition was performed in a BD FACSCanto II flow cytometer using BD FACSDiva software (both from BD Biosciences, San Jose, CA, USA). Analysis was performed using FlowJo V10 software (Tree Star, Ashland, OR, USA).

Immunofluorescence and confocal microscopy

For synapse studies, Jurkat NT-T, CAR-T19, and STAb-T19 cells were incubated for 15 minutes on Poly-L-lysine (Sigma-Aldrich)-coated coverslips at 37°C with Raji cells at a Jurkat:Raji ratio of 1:1. Where indicated, Raji cells were loaded for 1 hour with 5 nM BLI or 1 µg/mL SEE. In order to properly find cell conjugates, Raji cells were pre-incubated with the fluorescent tracker chloromethyl derivative of aminocoumarin (CMAC) 1 µM (Molecular Probes, Eugene, OR, USA). Jurkat:Raji cell conjugates (200,000 cells each) were fixed with 4% paraformaldehyde in PBS for 5 minutes at room temperature, permeabilized with 0.1% Triton X-100 (Sigma Aldrich) for 5 minutes at room temperature, and blocked with 10 µg/ml human gamma globulin (Sigma-Aldrich) for 20 minutes at room temperature. Samples were stained with mouse anti-CD3ε mAb (T3b clone; kindly provided by Dr. Francisco Sánchez-Madrid, Hospital Universitario de la Princesa, Madrid, Spain) and with Phalloidin-647 (Molecular Probes) (for F-actin detection) for 1 hour at room temperature. Cells were then washed with TBS (50 mM Tris-HCl, pH 7.4 150 mM NaCl) and incubated with an Alexa 488-conjugated GAM secondary antibody (Molecular Probes) at room temperature for 30 minutes. Finally, samples were washed with TBS and distilled water before being mounted with Mowiol medium (Sigma-Aldrich). Confocal sections of fixed samples were acquired using an SP-8 laser scanning confocal microscopy (Leica Microsystems, Wetzlar, Germany), with a 60×/1.35 oil immersion objective. CMAC, Alexa 488, and phalloidin-647 were excited by 405, 488, and 633 nm laser lines, respectively. Image acquisition was performed using a Leica HyVolution system and an automatically optimized image resolution of 40 nm/pixel. For 3D reconstructions, z-stacks through the complete IS were acquired every 0.3 µm. F-actin clearance was estimated by the ratio of the area of the central region of the IS depleted of F-actin versus the complete area of the IS including the actin ring in 3D images. Assessment of CD3 coalescence at the cSMAC was assessed by visual inspection of the 3D images and using criteria shown in supplementary Figure 2. 3D reconstruction and image quantitation were performed using ImageJ freeware (National Institutes of Health, Rockville, MD, USA).

For 19-CAR and CD3 localization studies, J-NT-T, J-CAR-T19, or J-STAb-T19 cells (1×10^5) were co-cultured for 2 hours with CMAC-labeled NALM6 cells at a 2:1 E:T

ratio in U-bottom 96-well plates. Co-cultures were then incubated on poly-L-lysine-coated coverslips at 37°C, 5% CO₂ and fixed and permeabilized as described above. 19-CAR localization at the lysosomal compartment was assessed by staining with GAMIgG F(ab')₂-biotin (Jackson ImmunoResearch) followed by streptavidin-Alexa Fluor 594 (Life Technologies-Thermo Fisher Scientific, Carlsbad, CA, USA) and mouse anti-CD107a (IDB4 clone)-Alexa Fluor 647 (Biolegend, San Diego, CA, USA). CD3 localization was determined by staining with mouse anti-CD3ε (T3b clone) followed by GAM-Alexa-488. All samples were mounted with Mowiol (Sigma-Aldrich) as described above. Confocal sections were acquired using the SP-8 scanning laser confocal microscopy equipped as described. CMAC, Alexa 488, Alexa 594, and Alexa 647 were excited by 405, 488, 594, or 633 nm laser lines, respectively. Image acquisition was automatically optimized with the Leica software to get an image resolution of 58 nm/pixel. In the case of 19-CAR localization, Z-stacks through the cell were acquired every 0.8 μm. Colocalization was estimated by Pearson correlation coefficients obtained in complete stacks of cells (Figure 2b, c). CD3ε uptake by target cells shown in Figure 3e was estimated as the ratio of the signal of CD3ε in NALM6 cells and JK cells after subtracting the background. Analysis was implemented in ImageJ freeware.

Statistical analysis

Results of experiments are expressed as mean ± standard deviation (SD). Graphics and the statistical tests indicated in figure legends were performed using Prism 6 (GraphPad Software, USA).

Results

Generation and characterization of anti-CD19 Jurkat CAR-T and STAb-T cells

Jurkat T cells were transduced at different multiplicities of infection (MOI) with lentiviruses encoding a second-generation (CD8-BBζ) anti-CD19 CAR (19-CAR) or an anti-CD19 × anti-CD3 BiTE (19-BiTE) (Figure 1a), and the relationship between the number of vector integrations and transgene expression was analyzed. Vector copy number (VCN) was found to be similar in both cases, between 1 and 5 copies for 19-CAR-transduced Jurkat T cells (J-CAR-T19) and between 1 and 7 for 19-BiTE-infected Jurkat T cells (J-STAb-T19) (Fig. S1a). The intracellular levels of both proteins were similar, as determined by Western blotting, with a clear correlation between MOI and both 19-CAR expression (Fig. S1b) and 19-BiTE expression and secretion (Fig. S1c,d). The percentage of 19-CAR-positive cells among J-CAR-T19 cells varied between 65% and 100% according to the VCN increase, and a VCN-dependent surface staining of J-STAb-T19 cells was observed as well, ranging from 16% to 78%, indicating that secreted 19-BiTEs were bound to the CD3 complexes on the T cell surface (Fig. S1e). Jurkat T cells transduced at MOI 5 were selected

for use in subsequent studies since VCN was <5 copies per genome in both J-CAR-T19 and J-STAb-T 19 cells, and the 19-CAR and 19-BiTE expression levels were homogeneous and stable.

Importantly, the process of cis-/trans-decoration of the TCR/CD3 complex by the secreted 19-BiTE (Figure 1a and Fig. S1e) results in specific adhesion of J-STAb-T19 cells to plastic immobilized CD19, almost as efficient as observed with 19-CAR expressing cells (Figure 1b). T cell activation was further reflected by expression of the activation marker CD69 when J-CAR-T19 or J-STAb-T19 cells were co-cultured with CD19⁺ target cells (Figure 1c).

Topology of the immune synapses induced by Jurkat CAR-T19 and STAb-T19 cells

To study the assembly of 19-CAR- and 19-BiTE-mediated IS, J-CAR-T19 and J-STAb-T19 cells were co-cultured with CD19-expressing Raji cells. As controls, non-transduced Jurkat cells (J-NT-T) were co-cultured with unloaded (non-activated control) or with BLI- or SEE-loaded Raji cells (activation controls). Jurkat:Raji cell conjugates were stained for filamentous (F)-actin and CD3ε to evaluate the organization of the distal and central supramolecular activation clusters, dSMAC and cSMAC, respectively. Confocal 3D microscopy was implemented to visualize the central F-actin clearance, with the typical actin ring at the dSMAC, and the coalescence of CD3ε microclusters at the cSMAC occurring in the mature IS (Fig. S2). All conditions, including CAR-T19 cells, recruited CD3ε to the IS. However, while J-STAb-T19 cells cleared F-actin and formed the cSMAC by CD3 coalescence in a similar way to J-NT-T cells stimulated by SEE or BLI, CAR-T19 cells formed a disorganized IS with disperse CD3 clusters and a diffuse organization of F-actin (Figure 1d-f). These data showed that 19-BiTE, but not 19-CAR, allows the organization of a canonical IS and confirm our previous results obtained with engineered primary T cells.²⁸

Early signaling during J-CAR-T19 and J-STAb-T19 cell activation

In order to assess if the differences observed in synapse topology might have functional consequences, the early signaling triggered upon J-CAR-T19 and J-STAb-T19 interaction with CD19⁺ Raji cells was studied. As activation controls, J-NT-T cells were stimulated with BLI- or SEE-loaded Raji cells. As negative control, J-NT-T cells were incubated with Raji cells alone. PLCγ1 and ERK1/2 activation was analyzed by Western blot due to their important role in early activation signaling downstream the TCR/CD3. Interestingly, J-STAb-T19 cells showed PLCγ1 and ERK1/2 activation kinetics similar to J-NT-T cells stimulated with SEE or BLI. However, J-CAR-T19 cells showed a more transient signaling compared to J-STAb-T19 cells and control stimulation conditions (Figure 1g,h and Fig. S3).

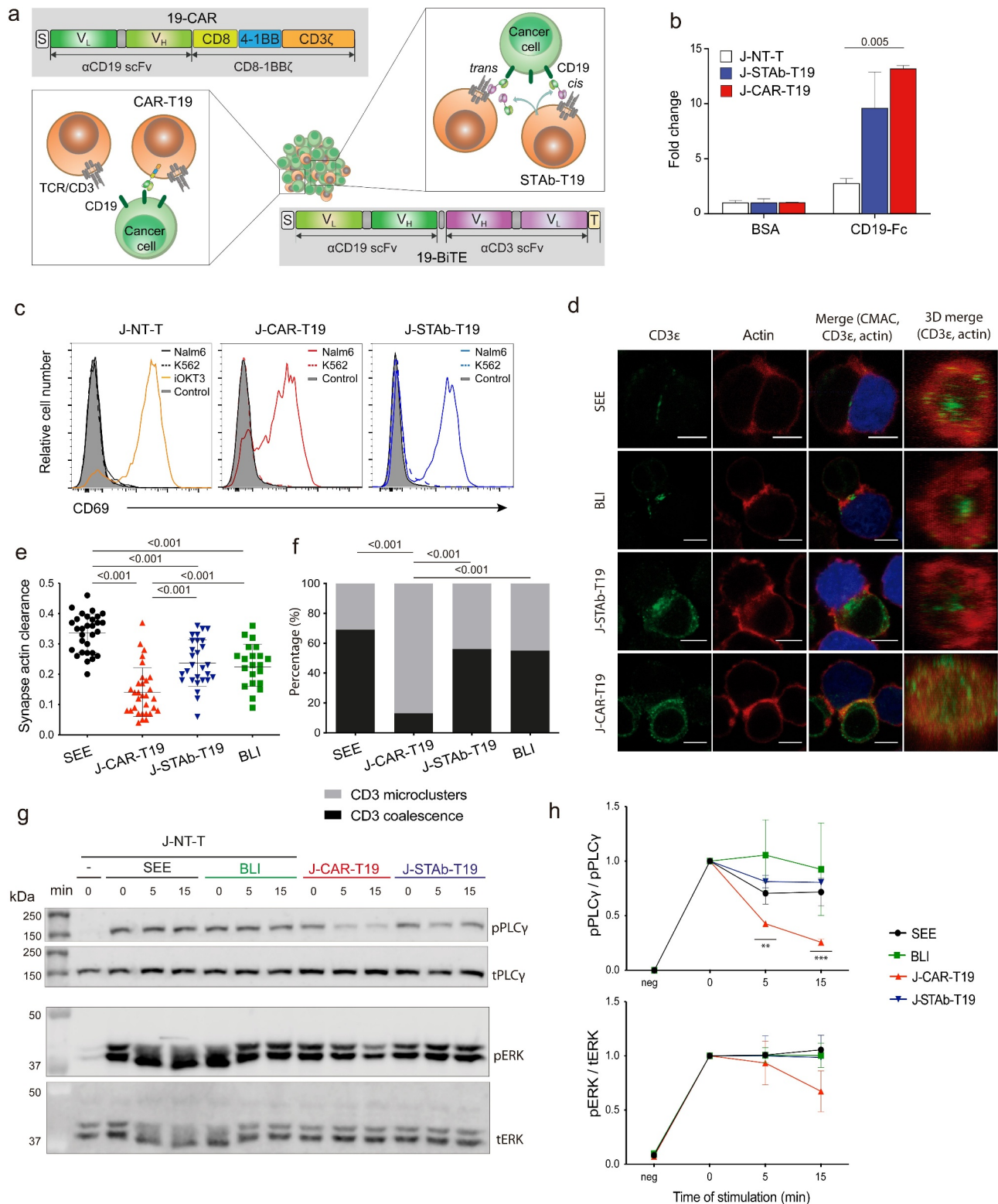


Figure 1. Functional characterization, IS assembly, and early signaling in J-CART19 and J-STAb-T19 cells. (a) Schematic representation of 19-CAR and 19-BiTE constructs and CAR-T19 and STAb-T19 cells. Whereas in the CAR-T strategy, only genetically engineered 19-CAR-expressing cells are able to interact with target cells, the 19-BiTE secreted by STAb-T cells can achieve a polyclonal recruitment of the complete T cell pool, including engineered and not engineered T cells. (b) Adhesion of J-NT-T, J-CAR-T19 and J-STAb-T19 cells to plastic-immobilized BSA or human CD19 (CD19-Fc). (c) CD69 expression by J-NT-T, J-CAR-T19 or J-STAb-T19 cells cocultured with CD19⁺ K562, CD19⁺ NALM6 target cells or plastic immobilized anti-CD3 mAb (iOKT3) for 24 hours. (d-h) J-NT-T, J-STAb-T19 and J-CAR-T19 cells were cocultured for the indicated minutes (min) with Raji cells. As activation controls, J-NT-T cells were incubated with CD19⁺ Raji cells loaded with SEE or blinatumomab 5 nM (BLI). (d) Distribution of CD3 ϵ and actin at the mature IS in representative cell conjugates of Jurkat cells interacting with Raji cells labelled with CMAC (blue). The green (CD3 ϵ) and red (actin) channels, as well as the merged images, are shown. Scale bar corresponds to 5 μ m. The IS topology obtained from the 3D reconstructions of region of interest placed at the IS in confocal stacks containing the red and the green channels are shown. (e) The graph represents the actin clearance at the IS in each sample, estimated as the fraction of actin cleared area as explained in material and methods. Symbols in each sample indicate individual cells analyzed and the black line the average value. Samples were compared by an ordinary one-way ANOVA with a Tukey's multiple comparison test. (f) Graph representing the percentage of cell conjugates showing peripheral CD3 microclusters or cSMAC formation by CD3 coalescence. Contingency tests were performed in each possible comparison. Analysis from three independent experiments is shown. (g) Western blot for quantification of PLC γ and ERK1/2 activation. (h) Phosphorylated fraction of the molecules analyzed in (g), normalized to the maximum fraction found in 0 minutes (min). Mean \pm SD from three independent experiments is shown. Samples were compared by a paired two-tailed Student t-test.

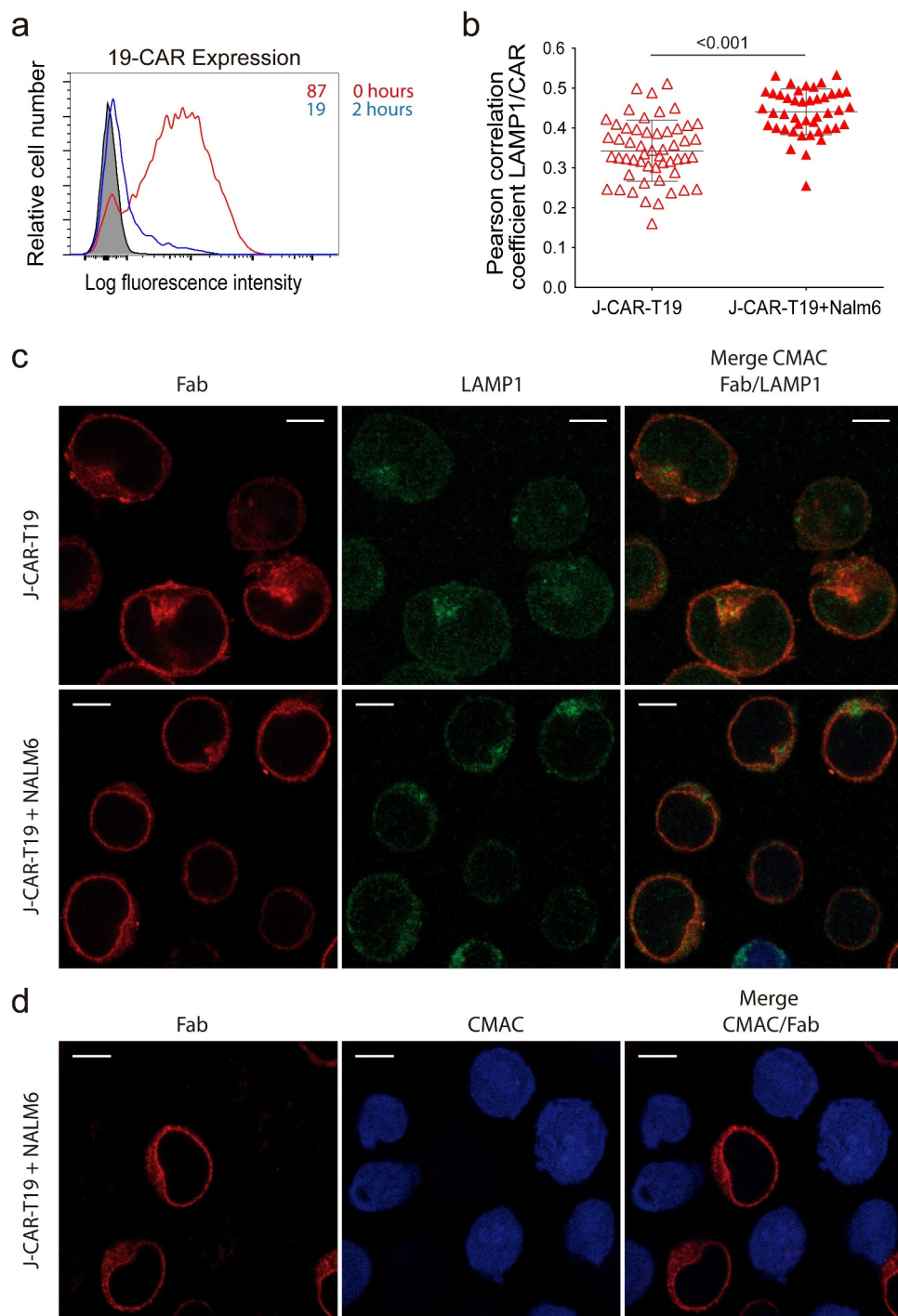


Figure 2. CAR downmodulation and fate upon antigen engagement. (a) J-CAR-T19 cells were co-cultured for 2 hours at a 2:1 E:T ratio with NALM6 cells and stained with an antimouse Fab antibody. 19-CAR expression by J-CAR-T19 cells before and after the coculture was analyzed by flow cytometry. Percentages of 19-CAR positive cells are indicated. (b-d) J-CAR-T19 cells and CMAC-labeled NALM6 cells were cocultured for 2 hours at 2:1 E:T ratio, stained with antibodies against mouse Fab and LAMP1, and analyzed by confocal microscopy. (b) Pearson's coefficients and (c) representative images of cellular colocalization of 19-CAR and LAMP1 in J-CAR-T19 cells after 2-hour culture. The green (LAMP1) and red (Fab) channels, as well as the merged images, are shown. The scale bar corresponds to 5 μm . Dots in graphs represent the Pearson's coefficient in the individual cells analyzed, and the black line the average value of one representative experiment out of two. Samples were compared by unpaired t-test. (d) Representative images showing the absence of 19-CAR uptake by NALM6 target cells. One experiment out of three is shown.

Modulation and trafficking of cell surface 19-CAR and CD3 molecules

Duration of signal transduction could also be related to the presence of adequate levels of the activating molecules on the T cell surface. Interestingly, as we had previously reported,²⁸ a rapid and drastic 19-CAR downmodulation occurs after

interaction with CD19⁺ cells (Figure 2a), which might account for the shorter signaling observed in J-CAR-T19 cells. In an attempt to define the fate of the 19-CAR molecules, J-CAR-T19 cells were cultured alone or with CD19⁺ NALM6 cells for 2 hours and co-stained with antibodies against mouse Fab (Fab), for 19-CAR detection, and against the lysosome-associated

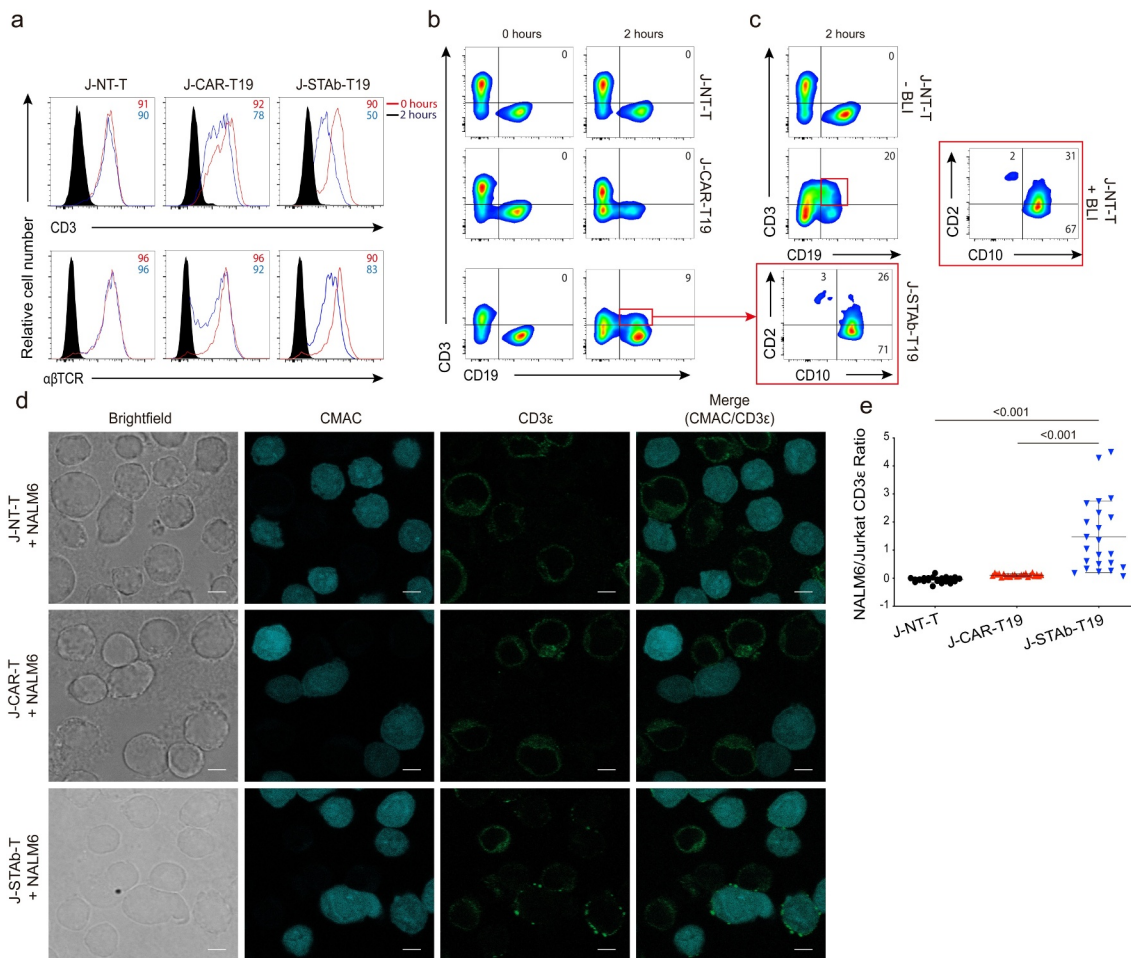


Figure 3. 19-BiTE-mediated CD3 uptake by target cells. (a,b) J-NT-T, J-CAR-T19 or J-STAb-T19 cells were co-cultured for 2 hours at a 2:1 E:T ratio with CMAC-labeled NALM6 cells. (a) Analysis, by flow cytometry, of CD3 and TCR expression on J-NT-T, J-CAR-T19 and J-STAb-T19 cells before and after the co-culture; one representative experiment out of three is shown. (b) Analysis of CD3/CD19 and CD2/CD10 co-expression at 0 and 2 hours after co-culture; one representative experiment out of three is shown. (c) J-NT-T cells were co-cultured for 2 hours at a 2:1 E:T ratio with CMAC-labeled NALM6 cells in the presence of 100 ng/ml BLI. CD3/CD19 and CD2/CD10 co-expression was analyzed before and after the coculture; one representative experiment out of three is shown. (d) Representative images of CD3 localization in both Jurkat and CMAC labeled-NALM6 cells after the coculture. The cyan (CMAC), green (CD3ε) and bright field channels, as well as the merged images of cyan and green, are shown. Scale bar corresponds to 5 μm. (e) Ratio of NALM6/Jurkat cell CD3 signal after 2 hours of co-culture. Dots represent the individual cells analyzed, and the black line the average value of one representative experiment out of two. Samples were compared by a one-way ANOVA with a Tukey's multiple comparison test.

membrane glycoprotein 1 (LAMP1). The analysis by confocal microscopy showed an increase in the colocalization of 19-CAR and LAMP1 in J-CAR-T19 cells cocultured with NALM6 cells, compared to J-CAR-T19 cells cultured alone (Figure 2b,c), indicating the traffic of 19-CAR to the lysosomal compartment after the interaction with the target antigen. 19-CAR was not detected on the cell surface nor in cellular compartments of CD19⁺ target cells after the coculture (Figure 2d), suggesting that 19-CAR downmodulation in J-CAR-T19 cells is not due to 19-CAR uptake by NALM6 cells upon interaction.

Following 19-BiTE-mediated engagement with CD19⁺ target cells, a reduced cell surface detection of CD3 was observed in J-STAb-T19 cells, which is more pronounced than that observed in J-CAR-T19 cells cocultured in the same conditions with NALM6 cells (Figure 3a). This cell surface CD3 decrease was concomitant with a modest TCR downmodulation (Figure 3b). Interestingly, the reduction in CD3 expression from J-STAb-T19 cells paralleled the increase in cell surface

detection of CD3 on NALM6 cells and the emergence of a CD19⁺CD10⁺CD3⁺ subpopulation, suggesting that CD3 is transferred to leukemia cells following 19-BiTE-mediated interactions (Figure 3b). The CD3 uptake by CD19⁺ target cells was also observed in cocultures of NALM6 cells with J-NT-T cells in the presence of BLI (Figure 3c). To further address these observations, J-NT-T, J-CAR-T19, or J-STAb-T19 cells were cocultured with CMAC-labeled NALM6 target cells for 2 hours, labeled with anti-CD3 mAb and analyzed by confocal microscopy. When co-cultured with J-STAb-T19 cells, CD3 aggregates were observed at the NALM6 cell surface, which were not observed when NALM6 was cocultured with J-NT-T or J-CAR-T19 cells (Figure 3d,e), suggesting that CD3 trogocytosis³⁵ occurred after the 19-BiTE-mediated interaction. This could explain, at least in part, the higher reduction in CD3 cell surface expression observed in J-STAb-T19 cells, compared to J-NT-T and J-CAR-T19 cells. On the other hand, a decrease in CD19 expression on NALM6 target cell surface upon interaction with J-CAR-T cells was observed (Figure 3b), as previously described.²⁸

Discussion

We have recently reported the generation of STAb-T19 cells secreting a previously uncharacterized anti-CD19 × anti-CD3 BiTE and demonstrated their potent antitumor activity in relevant *in vivo* B-ALL models when compared to CAR-T cells expressing a cell surface CD19-targeted second-generation CAR.²⁸ Interestingly, we observed significant differences in the topology of 19-CAR- and 19-BiTE-mediated synapses in human primary T lymphocytes. In the present study, we have performed a detailed analysis on the characteristics and potential outcomes of both types of anti-CD19-mediated target cell-T cell interactions. For this purpose, we have used the Jurkat human T cell line, which has been widely used to study T cell activation, signaling, and IS assembly.³⁶ Contrary to primary T cells, Jurkat cells can be easily expanded and long-term cultured after transduction without losing CAR expression or BiTE secretion, avoiding transduction-to-transduction differences and loss of transgene expression. In addition, clonal stimulation by superantigens provides a proper control that mimics the canonical IS and, together with the high transduction efficiency achieved in Jurkat cells, allows to perform experiments with a high number of T cell-target cell interactions. Jurkat cell stimulation with SEE and B-cell lines has been previously used for synapse studies,³⁷ and Jurkat cells have been employed to evaluate the CAR- and BsAb-induced IS and signaling in T cells.^{31,38}

Therefore, human Jurkat T cells were conveniently transduced with lentiviral vectors encoding 19-CAR or 19-BiTE, as determined by western blot and flow cytometry. Importantly, in 19-BiTE transduced STAb-T19 cells a VCN-dependent cell surface staining was observed with an anti-His-tag mAb, indicating that secreted 19-BiTEs are loaded onto the TCR/CD3 complexes on the T cell surface, and this process of “cis-/trans-CD3 decoration” results in an effective and specific adhesion of T cells to CD19-coated wells. To the best of our knowledge, this is the first report describing the ability of “BiTE-decorated” T cells to bind to human CD19, which would endow them with the ability to selectively target and kill CD19⁺ tumor cells *in vivo*.

TCR engagement leads to the formation of the IS, a highly organized structure composed of concentric SMACs, which must be finely tuned to achieve proper T cell activation and effective immune responses.^{39,40} The precise spatial and temporal topology of the IS assembled in response to CARs and BiTEs is poorly understood, but it has been reported that CAR-mediated synapse exhibited major differences relative to the typical TCR-initiated IS.^{26,40} Thus, previous studies have described a disorganized multifocal pattern, differing from the canonical “bull’s eye” structure in CAR-mediated IS,²⁶ and with a poor organization of the actin ring.⁴¹ Unlike CARs, small-sized T cells engaging bsAbs have been previously reported to induce the formation of a canonical IS between T lymphocytes and tumor cells.²⁹ Different bsAb formats have shown an efficient peripheral and central recruitment of F-actin and CD3 at the synapse, where proper polarization of TCR signaling is occurring.⁴² Indeed, BiTE-initiated IS has been found to be identical in structure and molecular composition to TCR-induced IS.^{30,31} Accordingly, our previous and

current results showed that F-actin is not properly cleared from the central area of interaction in J-CAR-T19 cells compared to conventional TCR-IS. In addition, J-CAR-T19 cells were able to recruit CD3 to the IS but failed to centralize it in the cSMAC. Importantly, a crucial event in synapse formation is the movement of TCR/CD3 microclusters to the inner SMAC (cSMAC).⁴³ Actin plays an important role in this centripetal movement of TCR microclusters,^{44–46} and the actin retrograde flow sustains the PLC γ 1 signaling,⁴⁷ which is a key step in the T cell activation process triggered by the TCR.^{48–50} Opposite to CAR-mediated synapse, 19-BiTE- and BLI-induced synapses are similar to those observed in the well-established RAJI-SEE-Jurkat IS model, which configures a canonical synapse,⁵¹ with actin clearance and CD3 accumulation in the cSMAC. Nevertheless, it should be noted that, although the dSMAC was formed in J-STAb-T19 cells and BLI-stimulated cells, the central area of the IS with low content of actin was smaller. Actin clearance is also important for the secretion of lytic granules or cytokines to the synaptic cleft.⁵² We envisage that actin networks organized at the IS induced in J-STAb-T19 cells will be ready for proper secretion of lytic granules in a similar way than the canonical IS organized in CTLs.

To determine the functional impact of such differences, we analyzed the activation of early T cell signaling pathways after coculture with CD19⁺ target cells. Data showed shorter signaling in J-CAR-T19 cells compared to control Raji-SEE-stimulated J-NT-T cells. This might be related to the observation that the time required for the CAR to assembly a functional IS is shorter than the time required by the TCR.²⁷ Thus, CAR-stimulated T cells dissociate faster than TCR-stimulated T cells from killed tumor targets, which may enable a more efficient serial killing.²⁶ However, rather than leading to more efficient tumor clearance, CAR-mediated killing was reduced compared to that mediated by TCR ligation.⁵³ This could be due to several reasons. First, because T cell exhaustion occurs after repeated T cell activation, we might speculate that the faster kinetics of serial killing would render CAR-T cells more rapidly prone to exhaustion. Second, the reduced killing capacity of CAR-T cells compared with TCR-stimulated T cells has been attributed to strong downregulation of CARs.⁵³

An important issue regarding target-T cell interactions is the dynamics of cell surface molecules that enable the TAA-specific recognition and activation of effector cells, since a low density of activation-triggering molecules might reduce the cytotoxic potential of redirected effectors. We had previously observed a fast and drastic 19-CAR downmodulation upon interaction with CD19 that has been confirmed in the present study. Analysis of 19-CAR location after co-culture with CD19⁺ target cells showed an increase of 19-CAR co-localization with the lysosomal marker LAMP1, which would be in accordance with the previously described lysosomal degradation of internalized 19-CARs.⁵⁴ In contrast, 19-BiTE-mediated interactions elicited signaling kinetics similar to those generated by TCR-mediated interactions. In addition, we found a reduction of cell-surface CD3 detection after STAb-T19 cell coculture with CD19⁺ cells. Such a reduction could be partially explained by epitope competition between 19-BiTE and the anti-CD3 mAb used for detection. On the other hand, CD3 downmodulation could obey the physiological dynamics of the TCR/CD3 during a

canonical antigen stimulation, in which a decrease in the cell surface-TCR/CD3 complex occurs after ligation due to prevention of recycling of internalized complexes.⁵⁵ Loss of CD3 might also be associated with trogocytosis, a process of intercellular and bidirectional transfer of plasma membrane fragments along with their associated molecules, frequently observed at the IS between APCs and T cells.³⁵ The transferred proteins can be internalized by the receiving cells or displayed on their cell surface.^{35,56,57} The transfer of CD3 observed in our work is consistent with seminal observations of the presence of TCR components at exosomes delivered to the synaptic cleft.^{58,59} In addition, antibody-mediated trogocytosis has been previously described⁶⁰ even by bsAbs.^{61–63} Moreover, bidirectional trogocytosis between B and T cells mediated by CD19 × CD3 bsAbs has been documented, and it might be a common phenomenon on T cell-redirecting bsAbs.⁶³ Consequences of trogocytic transfer are diverse, depending on the functions of proteins embedded in the transferred membrane patches, and can both enhance or suppress immune responses.⁶⁴ Nevertheless, it is indicative of a more physiological response, and further investigation on the potential relevance of 19-BiTE-mediated CD3 uptake by CD19⁺ target cells is required.

In summary, we have demonstrated that the topology of the IS induced by the 19-BiTE and the 19-CAR in primary T cells is reproduced in Jurkat T cells, providing us a useful model to perform further studies and precisely define the impact of the IS architecture on the functional capacity, cytotoxic potential, and persistence of CAR-T19 and STAb-T19 cells. In fact, we have shown for the first time that two different antibody-based T cell-redirecting molecules carrying the same anti-CD19 clone have opposite outcomes in terms of IS formation and signaling. Further studies on primary T lymphocytes will be necessary to validate these findings and to determine whether such differences could represent an advantage of STAb-T cells over CAR-T cells in cancer immunotherapy.

Acknowledgments

We thank the technical assistance of the fluorescence microscopy facility staff of the Complutense University of Madrid.

Disclosure statement

BB and LA-V are inventors on a patent related to STAb-T cell therapy, filed by the Fundación de Investigación 12 de Octubre, IDIBAPS/Hospital Clinic, and Fundación CRIS contra el Cáncer. LA-V is cofounder of Leadartis S.L., a spin-off focused on unrelated interest.

Funding

This work was supported by the Spanish Ministry of Science and Innovation (PID2020115444GB-I00 and RTC-2017-5944-1 to PR-N; and SAF2017-89437-P, PID2020-117323RB-I00, and PDC2021-121711-I00 to LA-V), partially supported by the European Regional Development Fund (ERDF); the Carlos III Health Institute (ISCIII, PI20/01030 to BB; and DTS20/00089 to LA-V), partially supported by the ERDF; the Spanish Association Against Cancer (AECC 19084 to LA-V; INNOV211832BLAN to B.B); and the CRIS Cancer Foundation (FCRIS-IFI-2018 and FCRIS-2021-0090 to LA-V). ISCIII-RICORS is supported within the Next Generation EU program (Plan de Recuperación, Transformación y Resiliencia). LD-A was supported by a Rio Hortega fellowship from the

ISCIII (CM20/00004). OA-S was supported by a PhD fellowship from the Complutense University of Madrid. CD-A was supported by a predoctoral fellowship from the Spanish Ministry of Science and Innovation (PRE2018-083445).

ORCID

Ángel Ramírez-Fernández  <http://orcid.org/0000-0002-3265-6878>

Óscar Aguilar-Sopeña  <http://orcid.org/0000-0002-2435-8598>

Pedro Roda-Navarro  <http://orcid.org/0000-0003-3799-8823>

Luis Álvarez-Vallina  <http://orcid.org/0000-0003-3053-6757>

Belén Blanco  <http://orcid.org/0000-0001-5085-7756>

References

- Blanco B, Compte M, Lykkemark S, Sanz L, Alvarez-Vallina L. T cell-redirecting strategies to 'STAB' tumors: beyond CARs and bispecific antibodies. *Trends Immunol.* 2019;40(3):243–257. doi:10.1016/j.it.2019.01.008.
- Barrett DM, Singh N, Porter DL, Grupp SA, June CH. Chimeric antigen receptor therapy for cancer. *Annu Rev Med.* 2014;65(1):333–347. doi:10.1146/annurev-med-060512-150254.
- Maude SL, Laetsch TW, Buechner J, Rives S, Boyer M, Bittencourt H, Bader P, Verneris MR, Stefanski HE, Myers GD. Tisagenlecleucel in children and young adults with B-cell lymphoblastic leukemia. *N Engl J Med.* 2018;378(5):439–448. doi:10.1056/NEJMoa1709866.
- Neelapu SS, Locke FL, Bartlett NL, Lekakis LJ, Miklos DB, Jacobson CA, Braunschweig I, Oluwole OO, Siddiqi T, Lin Y. Axicabtagene ciloleucel CAR T-cell therapy in refractory large B-cell lymphoma. *N Engl J Med.* 2017;377(26):2531–2544. doi:10.1056/NEJMoa1707447.
- Mullard A. FDA approves first BCMA-targeted CAR-T cell therapy. *Nat Rev Drug Discov.* 2021;20:332.
- Xu X, Sun Q, Liang X, Chen Z, Zhang X, Zhou X, Li M, Tu H, Liu Y, Tu S. Mechanisms of relapse after CD19 CAR T-cell therapy for acute lymphoblastic leukemia and its prevention and treatment strategies. *Front Immunol.* 2019;10:2664. doi:10.3389/fimmu.2019.02664.
- Alonso-Camino V, Harwood SL, Alvarez-Mendez A, Alvarez-Vallina L. Efficacy and toxicity management of CAR-T-cell immunotherapy: a matter of responsiveness control or tumour-specificity? *Biochem Soc Trans.* 2016;44(2):40611. doi:10.1042/BST20150286.
- Kontermann RE, Brinkmann U. Bispecific antibodies. *Drug Discov Today.* 2015;20(7):838–847. doi:10.1016/j.drudis.2015.02.008.
- Nunez-Prado N, Compte M, Harwood S, Alvarez-Mendez A, Lykkemark S, Sanz L, Álvarez-Vallina L. The coming of age of engineered multivalent antibodies. *Drug Discov Today.* 2015;20(5):588–594. doi:10.1016/j.drudis.2015.02.013.
- Przepiorka D, Ko CW, Deisseroth A, Yancey CL, Candau-Chacon R, Chiu HJ. FDA Approval: blinatumomab. *Clin Cancer Res.* 2015;21(18):4035–4039. doi:10.1158/1078-0432.CCR-15-0612.
- Blinatumomab approval expanded based on MRD. *Cancer Discov.* 2018;8(6):OF3. doi:10.1158/2159-8290.CD-NB2018-059.
- Lutterbuese R, Raum T, Kischel R, Hoffmann P, Mangold S, Rattel B. T cell-engaging BiTE antibodies specific for EGFR potently eliminate. *Proc Natl Acad Sci U S A.* 2010;107(28):12605–12610. doi:10.1073/pnas.1000976107.
- Kantarjian H, Stein A, Gokbuget N, Fielding AK, Schuh AC, Ribera JM. Blinatumomab versus chemotherapy for advanced acute lymphoblastic leukemia. *N Engl J Med.* 2017;376(9):836–847. doi:10.1056/NEJMoa1609783.
- Jabbour E, Dull J, Yilmaz M, Khoury JD, Ravandi F, Jain N. Outcome of patients with relapsed/refractory acute lymphoblastic leukemia after blinatumomab failure: no change in the level of CD19 expression. *Am J Hematol.* 2018;93(3):371–374. doi:10.1002/ajh.24987.

15. Goebeler ME, Knop S, Viardot A, Kufer P, Topp MS, Einsele H. Bispecific T-cell engager (BiTE) antibody construct blinatumomab for the treatment of patients with relapsed/refractory non-Hodgkin lymphoma: final results from a phase I study. *J Clin Oncol.* 2016;34(10):1104–1111. doi:10.1200/JCO.2014.59.1586.
16. Topp MS, Gokbuget N, Stein AS, Zugmaier G, O'Brien S, Bargou RC, Dombret H, Fielding AK, Hefner L, Larson RA. Safety and activity of blinatumomab for adult patients with relapsed or refractory B-precursor acute lymphoblastic leukaemia: a multicentre, single-arm, phase 2 study. *Lancet Oncol.* 2015;16(1):57–66. doi:10.1016/S1470-2045(14)71170-2.
17. Davis KL, Mackall CL. Immunotherapy for acute lymphoblastic leukemia: from famine to feast. *Blood Adv.* 2016;1(3):265–269. doi:10.1182/bloodadvances.2016000034.
18. Molina JC, Shah NN. CAR T cells better than BiTEs. *Blood Adv.* 2021;5(2):602–606. doi:10.1182/bloodadvances.2020003554.
19. Sanz L, Blanco B, Alvarez-Vallina L. Antibodies and gene therapy: teaching old 'magic bullets' new tricks. *Trends Immunol.* 2004;25(2):85–91. doi:10.1016/j.it.2003.12.001.
20. Alvarez-Vallina L. Genetic approaches for antigen-selective cell therapy. *Curr Gene Ther.* 2001;1(4):385–397. doi:10.2174/1566523013348418.
21. Compte M, Blanco B, Serrano F, Cuesta AM, Sanz L, Bernad A, Holliger P, Álvarez-Vallina L. Inhibition of tumor growth in vivo by in situ secretion of bispecific anti-CEA x anti-CD3 diabodies from lentivirally transduced human lymphocytes. *Cancer Gene Ther.* 2007;14(4):380–388. doi:10.1038/sj.cgt.7701021.
22. Velasquez MP, Torres D, Iwahori K, Kakarla S, Arber C, Rodriguez-Cruz T. T cells expressing CD19-specific engager molecules for the immunotherapy of CD19-positive malignancies. *Sci Rep.* 2016;6(1):27130. doi:10.1038/srep27130.
23. Liu X, Barrett DM, Jiang S, Fang C, Kalos M, Grupp SA, June CH, Zhao Y. Improved antileukemia activities of adoptively transferred T cells expressing bispecific T-cell engager in mice. *Blood Cancer J.* 2016;6(6):e430. doi:10.1038/bcj.2016.38.
24. Iwahori K, Kakarla S, Velasquez MP, Yu F, Yi Z, Gerken C, Song X-T, Gottschalk S. Engager T cells: a new class of antigen-specific T cells that redirect bystander T cells. *Mol Ther.* 2015;23(1):171–178. doi:10.1038/mt.2014.156.
25. Mukherjee M, Mace EM, Carisey AF, Ahmed N, Orange JS. Quantitative imaging approaches to study the CAR immunological synapse. *Mol Ther.* 2017;25(8):1757–1768. doi:10.1016/j.ymthe.2017.06.003.
26. Davenport AJ, Cross RS, Watson KA, Liao Y, Shi W, Prince HM, Beavis PA, Trapani JA, Kershaw MH, Ritchie DS. Chimeric antigen receptor T cells form nonclassical and potent immune synapses driving rapid cytotoxicity. *Proc Natl Acad Sci U S A.* 2018;115(9):E2068E2076. doi:10.1073/pnas.1716266115.
27. Watanabe K, Kuramitsu S, Posey AD Jr., June CH. Expanding the therapeutic window for CAR T cell therapy in solid tumors: the knowns and unknowns of CAR T cell biology. *Front Immunol.* 2018;9:2486. doi:10.3389/fimmu.2018.02486.
28. Blanco B, Ramirez-Fernandez A, Bueno C, Argemí-Muntadas L, Fuentes P, Aguilar-Sopeña O. Overcoming CAR-mediated CD19 downmodulation and leukemia relapse with T lymphocytes secreting anti-CD19 T cell engagers. *Cancer Immunol Res.* 2022. in press doi:10.1158/2326-6066.CIR-21-0853
29. Huehls AM, Coupet TA, Sentman CL. Bispecific T-cell engagers for cancer immunotherapy. *Immunol Cell Biol.* 2015;93(3):290–296. doi:10.1038/icb.2014.93.
30. Offner S, Hofmeister R, Romaniuk A, Kufer P, Baeuerle PA. Induction of regular cytolytic T cell synapses by bispecific single-chain antibody constructs on MHC class I-negative tumor cells. *Mol Immunol.* 2006;43(6):763–771. doi:10.1016/j.molimm.2005.03.007.
31. Kouhestani D, Geis M, Alsouri S, Bumm TGP, Einsele H, Sauer M, Stuhler G. Variant signaling topology at the cancer cell-T-cell interface induced by a two component T-cell engager. *Cell Mol Immunol.* 2021;18(6):1568–1570. doi:10.1038/s41423-020-0507-7.
32. Haryadi R, Ho S, Kok YJ, Pu HX, Zheng L, Pereira NA, Li B, Bi X, Goh L-T, Yang Y. Optimization of heavy chain and light chain signal peptides for high level expression of therapeutic antibodies in CHO cells. *PLoS One.* 2015;10(2):e0116878. doi:10.1371/journal.pone.0116878.
33. Castella M, Boronat A, Martín-Ibanez R, Rodriguez V, Sune G, Caballero M, Marzal B, Pérez-Amill L, Martín-Antonio B, Castaño J. Development of a novel anti-CD19 chimeric antigen receptor: a paradigm for an Affordable CAR T cell production at academic institutions. *Mol Ther Methods Clin Dev.* 2019;12:134–144. doi:10.1016/j.omtm.2018.11.010.
34. Compte M, Alvarez-Cienfuegos A, Nunez-Prado N, Sainz-Pastor N, BlancoToribio A, Pescador N, Sanz L, Álvarez-Vallina L. Functional comparison of single-chain and two chain anti-CD3-based bispecific antibodies in gene immunotherapy applications. *Oncoimmunology.* 2014;3(5):e28810. doi:10.4161/onci.28810.
35. Joly E, Hudrisier D. What is trogocytosis and what is its purpose? *Nat Immunol.* 2003;4(9):815. doi:10.1038/ni0903-815.
36. Cassioli C, Balint S, Compeer EB, Felce JH, Gamberucci A, Della BC, Felce SL, Brunetti J, Valvo S, Pende D. Increasing LFA-1 expression enhances immune synapse architecture and T cell receptor signaling in Jurkat E6.1 cells. *Front Cell Dev Biol.* 2021;9:673446. doi:10.3389/fcell.2021.673446.
37. Munoz P, Mittelbrunn M, de la Fuente H, Perez-Martinez M, Garcia-Perez A, Ariza-Veguillas A, Malavasi F, Zubiaur M, Sánchez-Madrid F, Sancho J. Antigen-induced clustering of surface CD38 and recruitment of intracellular CD38 to the immunologic synapse. *Blood.* 2008;111(7):3653–3664. doi:10.1182/blood-2007-07-101600.
38. Dong R, Libby KA, Blaeschke F, Fuchs W, Marson A, Vale RD, Su X. Rewired signaling network in T cells expressing the chimeric antigen receptor (CAR). *EMBO J.* 2020;39(16):e104730. doi:10.15252/embj.2020104730.
39. Soares H, Lasserre R, Alcover A. Orchestrating cytoskeleton and intracellular vesicle traffic to build functional immunological synapses. *Immunol Rev.* 2013;256(1):118–132. doi:10.1111/imr.12110.
40. Roda-Navarro P, Alvarez-Vallina L. Understanding the spatial topology of Artificial immunological synapses assembled in T cell-redirecting strategies: a major issue in cancer immunotherapy. *Front Cell Dev Biol.* 2019;7:370.
41. Xiong W, Chen Y, Kang X, Chen Z, Zheng P, Hsu YH, Jang JH, Qin L, Liu H, Dotti G. Immunological synapse predicts effectiveness of chimeric antigen receptor cells. *Mol Ther.* 2018;26(4):963–975. doi:10.1016/j.ymthe.2018.01.020.
42. Harwood SL, Alvarez-Cienfuegos A, Nunez-Prado N, Compte M, HernandezPerez S, Merino N, Bonet J, Navarro R, Van Bergen En Henegouwen PMP, Lykkemark S. ATTACK, a novel bispecific T cell-recruiting antibody with trivalent EGFR binding and monovalent CD3 binding for cancer immunotherapy. *Oncoimmunology.* 2017;7(1):e1377874. doi:10.1080/2162402X.2017.1377874.
43. Varma R, Campi G, Yokosuka T, Saito T, Dustin ML. T cell receptor-proximal signals are sustained in peripheral microclusters and terminated in the central supramolecular activation cluster. *Immunity.* 2006;25(1):117–127. doi:10.1016/j.immuni.2006.04.010.
44. Hashimoto-Tane A, Yokosuka T, Sakata-Sogawa K, Sakuma M, Ishihara C, Tokunaga M, Saito T. Dynein-driven transport of T cell receptor microclusters regulates immune synapse formation and T cell activation. *Immunity.* 2011;34(6):919–931. doi:10.1016/j.immuni.2011.05.012.
45. Yi J, Wu XS, Crites T, Hammer JA III, Pollard TD. Actin retrograde flow and actomyosin II arc contraction drive receptor cluster dynamics at the immunological synapse in Jurkat T cells. *Mol Biol Cell.* 2012;23(5):834–852. doi:10.1091/mbc.e11-08-0731.
46. Murugesan S, Hong J, Yi J, Li D, Beach JR, Shao L. Formin-generated actomyosin arcs propel T cell receptor microcluster movement at the immune synapse. *J Cell Biol.* 2016;215(3):383–399. doi:10.1083/jcb.201603080.

47. Babich A, Li S, O'Connor RS, Milone MC, Freedman BD, Burkhardt JK. F-actin polymerization and retrograde flow drive sustained PLC γ 1 signaling during T cell activation. *J Cell Biol.* 2012;197(6):775–787. doi:10.1083/jcb.201201018.
48. Desai DM, Newton ME, Kadlecik T, Weiss A. Stimulation of the phosphatidylinositol pathway can induce T-cell activation. *Nature.* 1990;348(6296):669. doi:10.1038/348066a0.
49. Bonvini E, DeBell KE, Veri MC, Graham L, Stoica B, Laborda J, Aman MJ, DiBaldassarre A, Miscia S, Rellahan BL. On the mechanism coupling phospholipase C γ 1 to the B- and T-cell antigen receptors. *Adv Enzyme Regul.* 2003;43(1):245–269. doi:10.1016/S0065-2571(02)00033-X.
50. Das V, Nal B, Dujeancourt A, Thoulouze MI, Galli T, Roux P, Dautry-Varsat A, Alcover A. Activation induced polarized recycling targets T cell antigen receptors to the immunological synapse; involvement of SNARE complexes. *Immunity.* 2004;20(5):577–588. doi:10.1016/S1074-7613(04)00106-2.
51. Montoya MC, Sancho D, Vicente-Manzanares M, Sanchez-Madrid F. Cell adhesion and polarity during immune interactions. *Immunol Rev.* 2002;186(1):6882. doi:10.1034/j.1600-065X.2002.18607.x.
52. Martin-Cofreces NB, Vicente-Manzanares M, Sanchez-Madrid F. Adhesive interactions delineate the topography of the immune synapse. *Front Cell Dev Biol.* 2018;6:149. doi:10.3389/fcell.2018.00149.
53. Davenport AJ, Jenkins MR, Cross RS, Yong CS, Prince HM, Ritchie DS, Trapani JA, Kershaw MH, Darcy PK, Neeson PJ. CAR-T cells inflict sequential killing of multiple tumor target cells. *Cancer Immunol Res.* 2015;3(5):483–494. doi:10.1158/2326-6066.CIR-15-0048.
54. Li W, Qiu S, Chen J, Jiang S, Chen W, Jiang J, Wang F, Si W, Shu Y, Wei P. Chimeric antigen receptor designed to prevent ubiquitination and downregulation showed durable antitumor efficacy. *Immunity.* 2020;53(2):456–470. doi:10.1016/j.immuni.2020.07.011.
55. Liu H, Rhodes M, Wiest DL, Vignali DA. On the dynamics of TCR:CD3 complex cell surface expression and downmodulation. *Immunity.* 2000;13(5):66575. doi:10.1016/S1074-7613(00)00066-2.
56. Zeng Q, Schwarz H. The role of trogocytosis in immune surveillance of Hodgkin lymphoma. *Oncoimmunology.* 2020;9(1):1781334. doi:10.1080/2162402X.2020.1781334.
57. Li G, Bethune MT, Wong S, Joglekar AV, Leonard MT, Wang JK, Kim JT, Cheng D, Peng S, Zaretsky JM. T cell antigen discovery via trogocytosis. *Nat Methods.* 2019;16(2):183–190. doi:10.1038/s41592-018-0305-7.
58. Peters PJ, Geuze HJ, Van der Donk HA, Slot JW, Griffith JM, Stam NJ, Clevers HC, Borst J. Molecules relevant for T cell-target cell interaction are present in cytolytic granules of human T lymphocytes. *Eur J Immunol.* 1989;19(8):1469–1475. doi:10.1002/eji.1830190819.
59. Peters PJ, Geuze HJ, Van der Donk HA, Borst J. A new model for lethal hit delivery by cytotoxic T lymphocytes. *Immunol Today.* 1990;11:28–32. doi:10.1016/0167-5699(90)90008-W.
60. Iwasaki S, Masuda S, Baba T, Tomaru U, Katsumata K, Kasahara M, Ishizu A. Plasma-dependent, antibody- and Fc γ 3 receptor-mediated translocation of CD8 molecules from T cells to monocytes. *Cytometry A.* 2011;79(1):46–56. doi:10.1002/cyto.a.20984.
61. Rossi EA, Chang CH, Goldenberg DM, Bachmann MP. Anti-CD22/CD20 bispecific antibody with enhanced trogocytosis for treatment of Lupus. *PLoS One.* 2014;9(5):e98315. doi:10.1371/journal.pone.0098315.
62. Vijayaraghavan S, Lipfert L, Chevalier K, Bushey BS, Henley B, Lenhart R, Sendeki J, Beqiri M, Millar HJ, Packman K. Amivantamab (JNJ-61186372), an Fc enhanced EGFR/cMet bispecific antibody, induces receptor downmodulation and antitumor activity by monocyte/macrophage trogocytosis. *Mol Cancer Ther.* 2020;19(10):2044–2056. doi:10.1158/1535-7163.MCT-20-0071.
63. Rossi EA, Rossi DL, Cardillo TM, Chang CH, Goldenberg DM. Redirected T cell killing of solid cancers targeted with an anti-CD3/Trop-2-bispecific antibody is enhanced in combination with interferon-alpha. *Mol Cancer Ther.* 2014;13(10):2341–2351. doi:10.1158/1535-7163.MCT-14-0345.
64. Ahmed KA, Munegowda MA, Xie Y, Xiang J. Intercellular trogocytosis plays an important role in modulation of immune responses. *Cell Mol Immunol.* 2008;5(4):261–9, 718. doi:10.1038/cmi.2008.32.